Green Chemistry

Cutting-edge research for a greener sustainable future

Accepted Manuscript

Green Chemistry

Cutting-edge research for a greener sustainable future

rsc.li/greenchem

Volume 20
Number 9
7 May 2018
Pages 1919-2160

ISSN 1463-9262

ROYAL SOCIETY OF CHEMISTRY

PAPER
Paul T. Anastas et al.
The Green ChemisTREE: 20 years after taking root with the 12 principles

This is an Accepted Manuscript, which has been through the Royal Society of Chemistry peer review process and has been accepted for publication.

Accepted Manuscripts are published online shortly after acceptance, before technical editing, formatting and proof reading. Using this free service, authors can make their results available to the community, in citable form, before we publish the edited article. We will replace this Accepted Manuscript with the edited and formatted Advance Article as soon as it is available.

You can find more information about Accepted Manuscripts in the Information for Authors.

ROYAL SOCIETY OF CHEMISTRY

rsc.li/greenchem

Green Chemistry

Copper-based catalysts with tunable acidic and basic sites for selective conversion of levulinic acid/ester to γ-valerolactone or 1,4-pentanediol

Yuewen Shao[a], Kai Sun[a], Qingyin Li[a], Qianhe Liu[a], Shu Zhang[b], Qing Liu[c], Guangzhi Hu[d],*, Xun Hu[a],*

[a]School of Material Science and Engineering, University of Jinan, Jinan, 250022, P. R. China.

[b]College of Materials Science and Engineering, Nanjing Forestry University, Nanjing, 210037, P. R. China

[c]Key Laboratory of Low Carbon Energy and Chemical Engineering, College of Chemical and Environmental Engineering, Shandong University of Science and Technology, Qingdao 266590, P. R. China

[d]School of Chemical Science and Technology, Yunnan University, Kunming 650091, P. R. China

*Corresponding author. Tel. /fax: +86–531–89736201; E-mail: mse_hux@ujn.edu.cn (X. Hu); guangzhihu@ynu.edu.cn (G. Hu).

Submit to

Green Chemistry

For consideration for publication

Abstract: γ-Valerolactone (GVL) and 1,4-pentanediol (1,4-PDO) are the value-added chemicals that can be produced from levulinic acid/ester via hydrogenation coupled with acid/base-catalyzed reactions. In this study, we have demonstrated that the Cu-based catalysts produced via the hydrotalcite precursors with tunable distribution of acidic and basic sites could, according to the requirement of the targeting products, effectively tune the selectivity of GVL or to 1,4-PDO from levulinic acid/ester. The abundant Brønsted acidic sites over the CuAl catalyst suppressed the opening of the ring of GVL, achieving a higher GVL selectivity while inhibiting 1,4-PDO formation. The introduction of Mg species to the catalyst significantly increased the abundance of the basic sites on surface of the catalyst, which was essential for the selective conversion of GVL to 1,4-PDO via the opening of the ring structure of GVL, the rate-determining step from levulinic acid/ester to 1,4-PDO. In addition, the CuMgAl catalyst showed a much superior catalytic stability to the CuMg or CuAl catalyst due to the more stable crystal structure, the more developed porous structure, the higher dispersion of Cu species and the higher capability to suppress the growing of metallic Cu species under the hydrothermal conditions.

Keywords: Levulinic acid/ester; γ-valerolactone; 1,4-pentanediol; copper-based catalysts; hydrogenation.

1. Introduction

Conversion of renewable and abundantly available biomass into chemicals and bio-fuels has drawn increasing attention in recent years [1–3]. Levulinic acid (LA), a compound derived from hydrolysis of biomass, is a platform chemical for manufacturing other value-added chemicals due to its tunable functionalities [4,5]. Much effort has been made for conversion of LA to the highly valuable products such as levulinic esters [6,7], γ-valerolactone (GVL) [8,9], 1,4-pentanediol (1,4-PDO) [10,11], and other chemicals with versatile applications [12]. Among these chemicals, GVL can be applied to the fields of agriculture and cosmetics [13−15], and 1,4-PDO can also be a raw material for the synthesis of polyesters and other chemicals as well as biofuels [16,17].

LA contains a carbonyl and a carboxyl group. The hydrogenation of the carbonyl functionality to 4-hydroxyvaleric acid (4-HVA) coupled with the subsequent intramolecular dehydration reaction forms GVL with the ring structure [18,19]. The further hydrogenation of the carbonyl functionality in GVL and the opening ring with the hydrogenation produces 1,4-PDO [16,20], as shown in Scheme 1. To date, much effort has been devoted to the synthesis of GVL from LA via the development of various types of hydrogenation catalysts [21−28]. Among the catalysts developed, noble metal catalysts were regarded as more preferable for GVL conversion, due to their higher catalytic activity. For instance, Pt-Mo bimetallic catalyst [10], few-layer graphene-supported ruthenium catalysts [29] and supported Ruthenium catalysts [30], have been developed for the production of GVL and 1,4-PDO. However, from the prospect of industrial application, the use of the noble metal-based catalysts is not preferable, mainly originating from their high manufacturing cost. Development of the transition metal-based catalysts with the comparable catalytic activity to the noble metal catalysts is highly desirable as this could substantially reduce the cost in application. Hence, the Cu or Ni-based catalysts have been widely investigated for hydrogenation of levulinic acid/esters [31−33].

Except for the active metal sites of Cu or Ni for activating hydrogen and the chemical bonds, the acid/base properties of support are also crucial for achieving high

hydrogenation efficiency or tuning the selectivity of targeting products. For instance, Zhang and co-workers studied boron nitride-supported Pt catalysts for the selective hydrogenation of cinnamaldehyde to cinnamyl alcohol, and few acid-base sites exhibited a high cinnamyl alcohol selectivity [34]. Cui et al. investigated ternary synergistic catalysis of Cu and acid-base sites for hydrogenation of dimethyl oxalate to ethylene glycol, confirming that the precise control between metal and acid-base sites might be responsible for the selective hydrogenation or hydrogenolysis of C=O/C−O group [35]. Wu et al. reported that copper-based bifunctional nanocatalysts were selective for the hydrogenation of lactones to synthesize diols, and the roles of metal Cu and basic sites were studied [28]. These previous results clearly indicated the importance of acid-base sites in determination of the catalytic activity and selectivity in hydrogenation of organics [36,37]. The conversion of levulinic acid/ester to GVL or 1,4-PDO also involves the coordination or hydrogenation reaction and acid/base-catalyzed reactions. Therefore, we have developed a series of CuMgAl catalysts with tunable acidic/basic sites for the hydrogenation of levulinic acid/ester to probe the impacts of acidic/basic sites on the reaction network.

Our results demonstrated that GVL with the yield of 95.6% and 1,4-PDO with the yield of 99% can be achieved with levulinic acid/ester as the reaction substrate, as indicated in Scheme 1. This process can be tuned to produce either GVL or 1,4-PDO as the main product. The selective production of GVL can be attributed to the coordination between the metallic Cu sites and acidic sites, while the high yield of 1,4-PDO was due to the synergistic effect between the metal Cu particles and basic sites. Therefore, Cu-based catalysts with tunable acidic/basic sites can exhibit remarkable catalytic activity towards the conversion of levulinic acid/ester.

2. Materials and Methods

2.1. Feedstock materials

$Cu(NO_3)_2 \cdot 6H_2O$, $Mg(NO_3)_2 \cdot 6H_2O$, NaOH and Na_2CO_3 were purchased from Sinopharm Chemical Reagent Co., Ltd. LA, ethyl levulinate (EL) and $Al(NO_3)_3 \cdot 9H_2O$ were obtained from Shanghai Macklin Biochemical Co., Ltd. Lanthanum

trifluoromethanesulfonate (LTMS) was purchased from Shanghai Aladdin biochemical technology Co., Ltd. All reagents used herein were analytical grade and were used directly without further pretreatment. Besides, the commercial solid acid catalyst (D008) used in this study was purchased from Cary Environmental Technology Co., Ltd, and its specific parameter can be referred in our previous work [38].

2.2. Catalyst synthesis

Three samples of copper-based Layered Double Hydroxides (LDHs) with Cu/Mg molar ratios of 1 : 4, 1 : 2 or 1 : 1 were synthesized via a co-precipitation method and were named as CuMgAl-1-4, CuMgAl-1-2 as well as CuMgAl-1-1 in the text. The molar ratios of $(Cu + Mg)/Al$ were maintained at 3 to obtain the LDHs structure [39]. Typically, the total concentration of Cu and Mg in the solution was 0.75 mol/L, and the concentration of Al was 0.25 mol/L. In addition, CuMg (Cu^{2+}: 0.25mol/L; Mg^{2+}: 0.5 mol/L) and CuAl (Cu^{2+}: 0.375 mol/L; Al^{3+}: 0.25 mol/L) catalysts were also prepared for comparison. Typically, two aqueous solutions, one containing given amounts of metal nitrates [$Cu(NO_3)_2 \cdot 6H_2O$, $Mg(NO_3)_2 \cdot 6H_2O$ and/or $Al(NO_3)_3 \cdot 9H_2O$] and the other containing the precipitating agent, NaOH (4.0 mol/L), were dropped slowly into Na_2CO_3 solution (0.125 mol/L) while the pH value was maintained at around 9 at 40°C. After the precipitation, the temperature was increased to 65°C and stirred at this temperature for 30 min for crystallization, and then the mixture was aged at 65°C for 24 h. The precipitate was further washed with deionized water until the filtrate became neutral. The obtained samples were then dried at 80°C overnight, ground to fine powders and calcined at 500°C in a muffle furnace for 6 h in static air. The calcined samples were further reduced at 300°C for 2 h with a H_2 flow rate of 60 mL/min and a N_2 flow rate of 60 mL/min before catalyzing the hydrogenation reaction.

2.3. Catalysts characterizations

Crystallinity of the copper based catalysts was characterized with Rigaku Ultima IV X-ray diffraction spectrometer (XRD). A Cu target (K α-radiation source, $\lambda = 1.5406$ Å) was used and the scanning rate was 20 °/min with a scanning range from 5 to 80°.

The particle size was determined via the Debye-Scherrer equation.

The specific area of the calcined copper based catalysts was characterized by N_2 adsorption-desorption measurement at 77 K by using the Brunauer-Emmet-Teller (BET) method with the instrument of Biaode SSA–6000. Before the N_2 adsorption, the catalysts were degassed at 120°C for 120 min to remove the physically absorbed moisture.

The acidic/basic properties of the samples were evaluated by temperature programmed desorption (Biaode PCA-1200 instrument) with NH_3 and CO_2 as the probing molecule (NH_3−TPD and CO_2−TPD), respectively. Before the absorption, 100 mg of catalysts was degassed at 150°C for 30 min under a constant helium flow (20 mL/min), and then the sample was cooled to 50°C, and a flow of NH_3 or CO_2 (20 mL/min) was introduced for the adsorption for 1 h. Furthermore, helium was purged for 1 h at 20 mL/min to remove the physically absorbed NH_3 or CO_2 on/in the sample. Finally, the sample was heated from 50 to 800°C with a ramping rate of 20°C/min under a constant helium flow (20 mL/min). The desorbed ammonia or CO_2 was measured by a thermal conductivity detector (TCD).

The temperature programmed reduction in hydrogen (H_2-TPR) was performed to measure the reduction behaviors of the calcined Cu-based catalysts. Approximate 10 mg of catalysts were used, and the H_2-TPR tests were carried out on Vodo VDSorb 91x instrument by using a 5% H_2/Ar mixed gas with a flow rate of 10 mL/min at a ramping rate of 20 °C/min. The samples were heated from room temperature to 700°C and the signal changes were recorded by using a thermal conductivity detector (TCD). Besides, the reduction degree was calculated according to the consumption of H_2.

Transmission electron microscopy (TEM) was used to observe the morphology of fresh and spent catalysts to probe the microstructure and research the Cu particles size in different catalysts. The tests were carried out on the JEOL 2010 instrument. The samples were ultrasonically dispersed into ethanol firstly, and the supernatant was added on copper mesh for the analysis.

In-situ Diffuse Reflectance Infrared Fourier Transform Spectroscopy (DRIFTS) was employed for obtaining pyridine-Fourier Transform infrared (Py-FTIR) spectra via

temperature programmed desorption of pyridine to study Brønsted and Lewis acid sites of different catalysts. The characterization was performed on a Nicolet iS50 spectrometer equipped with a liquid–nitrogen–cooled MCT detector and a modified Harrick Praying Mantis DRIFT cell. The reduced Cu-based catalysts were ground uniformly and placed in the DRIFT cell. Before the analysis, the sample was firstly vacuumed at 200°C for 30 min, and the background was scanned. Pyridine was introduced into the DRIFT cell by N_2 bubbling (50 mL/min, 35°C) for 30 min. After pyridine absorption, the catalysts were further purged with N_2 at room temperature for 30 min, and then the catalysts were heated to 500°C at a ramping rate of 10 °C/min.

The morphology and elemental component of fresh and used Cu-based catalysts were recorded on a scanning electron microscope with energy-dispersive X-ray (EDX) spectrometry (SEM; FEI QUANTA FEG 250). X-ray photoelectron spectroscopy (XPS, Thermo Scientific Escalab 250Xi) was also performed for probing the elemental chemical states of surface Cu species on the spent and used catalysts.

The dispersions of copper and specific surface areas in the different catalysts were determined by N_2O chemisorption and H_2-TPR reverse titration with Vodo VDSorb 91x instrument. Before the measurement, the sample was pretreated at 120°C for 1 h under Ar flow (40.0 mL/min), and then reduced in a H_2/Ar flow (40.0 mL/min) at 300°C for 1 h. After that, the sample was flushed under Ar flow (40.0 mL/min) for 30 min, and then the temperature was cooled down to 60°C. N_2O was used for the oxidization of surface Cu atoms to Cu_2O with a flow of 40.0 mL/min for 1.0 h. Afterwards, the further reduction of Cu_2O was performed under H_2/Ar flow (40.0 mL/min), and the temperature was increased from 60 to 300°C with a ramping rate of 5 °C/min. Finally, the surface area and dispersions of copper species were measured according to the previous literature [28,35].

2.4. Catalytic test

The catalytic experiments were performed in an autoclave reactor with a volume of 10 mL. Typically, catalysts and substrate-solvent mixture (a total mass of 4 g) were loaded to the reactor vessel at room temperature, and the reactor was then purged initially with H_2 for three times and charged with H_2 to specific pressure. The reactor was then heated to the setting temperature within ca. 30 min with a stirring rate of 400 rpm. When reaching the reaction temperature, the reactor was maintained at this temperature for a specified reaction time. After finishing the reaction, the liquid products were collected for further characterization and the spent catalyst was centrifuged, washed with ethanol, and dried at 40°C in vacuum drying oven overnight for the further cycle experiments or characterizations.

2.5. *Analysis of the liquid samples*

The yields of liquid products and conversion of substrate were analyzed by a gas chromatography coupling with a mass spectrometer (GC–MS, Shimadzu GC−MS−QP 2020 instrument) equipped with a Wax pillar column (30 m of length, 0.25 mm of internal diameter, 0.25 μm of film thickness). Before the analysis, the liquid products were diluted to ca. 2 wt% in acetone, and the mixture of 0.5 μL was injected into the injection port with a split ratio of 50 : 1. The column temperature was initially maintained at 50°C for 3 min and then heated to 250°C at a ramping rate of 20 °C/min and hold at 250°C for 10 min using helium as the carrier gas. The target products were identified by the standard spectra of the National Institute of Standards and Technology library (NIST 2014).

The yield of liquid products is defined with the following equations:

$$\text{Yield (\%)} = \frac{\text{Mole of product produced}}{\text{Mole of reactant loaded}} \times 100\% \qquad \text{Eq. (1)}$$

The conversion of reactant is defined with the following equations:

$$\text{Conversion}\left(\%\right) = \frac{\text{Mole of reactant converted}}{\text{Mole of reactant loaded}} \times 100\% \qquad \text{Eq. (2)}$$

The turn over frequency (TOF) of conversion of reactant was determined when the conversion of reactant was below 20%. GVL was used as the reactant to calculate the TOF value, as its conversion can be controlled below 20% and it can account for the synergistic effect between metal Cu and basic sites. The TOF value represents the moles of reactant converted per hour over per mole metal Cu on the surface of catalyst, and it is defined shown in the following equations:

$$\text{TOF}\left(\text{h}^{-1}\right) = \frac{\text{Mole of reactant converted}}{\text{Mole of metal Cu on the surface of catalyst} \times \text{reaction time}} \qquad \text{Eq. (3)}$$

3.   Results and discussion

3.1. *Characterizations of Catalysts*

3.1.1   *XRD*

The X-ray diffraction (XRD) patterns of the CuMgAl catalysts were displayed in Fig. 1. The LDHs structures were formed in the co-existence of Cu, Mg and Al in formulation of the catalysts. As shown in Fig. 1a, the X-ray diffraction peaks at $2\theta =$ 11.3°, 22.8°, 34.7°, 39.1°, 46.4°, 60.6° and 61.9° were respectively assigned to (003), (006), (012), (015), (018), (110) and (113) crystal planes of hydrotalcite [JCPDS 35-0965]. After calcination at 500°C, the hydrotalcite structures were destroyed (Fig. 1b), and MgO and CuO became the major phases. Nevertheless, the CuO phase in CuMgAl-1-4, CuMgAl-1-2 and CuMg was not observed, indicating the high dispersion of CuO in the catalysts. The diffraction peaks of CuO, however, were present in CuMgAl-1-1 and CuAl catalysts.

After the reduction, the samples were also characterized by XRD, as shown in Fig. 1c. The metallic Cu with the diffraction peaks at $2\theta =$ 43.3°, 50.4° and 74.1°, attributing to the (110), (200) and (220) crystal planes of Cu phase [JCPDS 85-1326], was detected in all catalysts. The grain size of metallic Cu (Table 1) increased from 4.5 to 5.5 nm

with the increasing molar ratio of Cu/Mg in CuMgAl catalysts. In the CuAl catalyst without the presence of Mg, the grain size of Cu reached 12.9 nm, while the particle size of Cu was only 4.1 nm in the CuMg catalyst. Obviously, the presence of Mg played an important role to disperse Cu species. The impacts of Mg addition or the LDHs structure formation on the porous structure of the catalysts were further investigated with N_2 physical absorption/desorption.

3.1.2 N_2 physical absorption/desorption

Table 1 showed the specific area, pore volume and pore size of the calcined catalysts. The CuAl catalyst showed the lowest specific area and pore volumes than that of the catalysts containing Mg species, which was the reason for the higher crystallinity of Cu and particle size (Fig. 1c and Table 1). In addition, the presence of Mg in the catalyst formulation could also enhance the formation of the mesoporous structures. As shown in Fig. S1b, the pore semidiameters of the CuAl catalyst dispersed in a wide range (from ca. 1 to 50 nm). With the addition of Mg to the catalyst formulation, the dispersion of the pore semidiameters became more concentrated (from ca. 2 to 20 nm). The N_2 adsorption-desorption isotherms of the catalyst were assigned to type Ⅳ isotherms with H3-type hysteresisloops (Fig S1 a). To observe the microstructures of the catalysts, SEM and TEM characterizations were subsequently carried out.

3.1.3 SEM and EDX

As shown in Fig. S2, the different catalysts exhibit various microstructures. CuMgAl catalysts have flower-like structure, as the nature of LDHs was maintained at the reduced CuMgAl catalysts, which should be responsible for the bigger specific surface area (Table 1, Entries 2 to 4). As CuMgAl-1-2 exhibited obvious flower-like structure than other catalysts, and highest surface area was obtained over this catalyst. CuAl catalyst exhibited the agglomeration of blocks, and it might result in the lowest surface area, biggest particle sizes and smallest pore volume. The results of SEM can reflect the microstructures of different samples, and EDX characterization was also preformed to probe chemical composition of different catalysts and the elemental

mappings of Mg, Al, Cu and O. The chemical composition was shown in Table S1, and CuAl catalyst has highest Cu content than other catalysts, which might be due to strong interaction between Cu and Al and will be further discussed. As shown in Fig. S3, different elements uniformly dispersed in CuMgAl-1-2 and CuMgAl-1-1 catalysts. To further characterize the dispersion of Cu particles and morphology, TEM was also performed.

3.1.4 TEM and N_2O chemisorption

The TEM images are shown in Fig. S4, and CuMgAl-1-1 as well as CuMg catalysts exhibit sheet structure and Cu nanoparticles were highly dispersed on the carrier. However, CuAl catalyst possesses the bigger particles size comparing with the former, and it was due to the sintering and agglomeration of Cu particles, which can keep consistent with the results of XRD characterization. Besides, the sintering of Cu particles might affect the surface Cu dispersion (D_{Cu}) and surface area (S_{Cu}) and it was further characterized. N_2O chemisorptions results are shown in Table 1 and it indicated that lower dispersion and surface area was present in CuAl catalyst due to its sintering and agglomeration of Cu particle. Besides, higher copper loading can result in the decrease of Cu dispersion and surface area. The particles size and various constituents might affect the reduction performance of Cu-based catalysts, and the samples will be further characterized by H_2-TPR.

3.1.5 H_2-TPR

Fig. 2 shows the reduction profiles of copper oxide in the catalysts, and the reduction degree was shown in Table S1. One broad hydrogen consumption peak with varied peaking temperatures was observed for all the catalysts, which was attributed to the reduction of the CuO species to Cu, The hydrogen consumption peak of CuMg was centered at 269°C, which was lower than that of CuMgAl catalyst and was much lower than that of CuAl catalyst with the reduction peak of 289 and 316°C. Obviously, the presence of Al species in the catalyst promoted the interaction with CuO, and higher reduction degree was obtained in CuMg catalyst rather than in that catalyst with the

introduction of Al. In addition, as shown in Table 1, the particles size of Cu reduced in the CuAl catalyst was bigger than that in other catalysts, which also contributed to the upwards shift of the main reduction temperature [40], as smaller size of CuO is easier to be reduced and bigger size of CuO is difficult to be reduced, confirming that Al species in the catalyst promoted the interaction with CuO. Therefore, CuMgAl-1-1 and CuAl catalyst with more Al content can produce two reduction peaks, and one peak at low temperature was due to the reduction of highly dispersed Cu particles; the other peak at high temperature was attributed to the reduction of small size crystalline CuO [41]. The varied formulation of the catalysts also impacted the distribution of the acid/basic sites on the surface of catalyst, which was further investigated with NH_3/CO_2-TPD and pyridine-FTIR characterizations.

3.1.6   NH₃-TPD, Pyridine-FTIR and CO₂-TPD

To qualitatively and quantitatively characterize the surface acidity of Cu-based catalysts, NH_3-TPD and pyridine-FTIR were carried out. Fig. 3a and Table 2 show the NH_3-TPD results of the reduced catalysts. Moderate and strong acid sites, with the desorption temperature range of 250 to 400 and more than 400°C, could be identified for CuMgAl and CuAl catalysts with the exception of CuMg catalyst [42]. CuAl catalyst possessed higher acid amounts than other catalysts, originating from the alumina species in the catalysts. To further probe the types of acidic sites, Pyridine-FTIR characterization was further performed, as shown in Fig. 4. Abundant Brønsted and Lewis acid sites were detected in CuAl and CuMgAl-1-1 catalyst, and Lewis acid site was the main acidic sites with the increase of Mg content. Pyridine-FTIR spectra of CuMgAl-1-1 and CuAl catalysts were also recorded by temperature programmed desorption of pyridine, as shown in Fig. 4 (b) to (e). Lewis acid sites (1445 cm^{-1}) declined with the increase of desorption temperature, and it was still present even though desorption was coming to 500°C, confirming that strong acid sites are predominant in CuAl and CuMgAl-1-1 catalysts, which might be responsible for its activity [35].

MgO is an alkaline oxide, the addition of which neutralized the acidic sites. As

indicated in Table 2, the total amount of acidic sites decreased versus the increase of the content of MgO in the catalysts except for CuMgAl-1-1 catalyst. Correspondingly, the addition of MgO enhanced the abundance of the basic sites (Table 2), especially the basic sites with medium strength (ranging from 150 to 400°C) (Fig. 3b) [43], and CuMgAl-1-1 and CuMg catalysts possess more basic sites than other CuMgAl catalysts. The effects of the drastically distinct distribution of the acidic/basic sites on activity/selectivity of the catalysts were further investigated.

3.2. Catalytic Activity

Table 3 shows the results for the hydrogenation of levulinic acid with ethanol as the reaction medium. The highest yield of GVL was obtained over the CuAl catalyst (Table 3, Entry 4). Besides, the reaction intermediate like 4-hydroxyvaleric acid (4-HVA) was present over there catalysts at 110°C, as the previous work indicated that the lactonization of 4-hydroxyvaleric acid was the rate-determining step [44]. The further increase of the reaction temperature from 110 to 170°C did not further promote the formation of GVL, but promoted the production of 1,4-PDO via the opening ring of GVL and the subsequent hydrogenation, especially for that over CuMg catalysts. The production of GVL from the lactonization of 4-HVA, the hydrogenation product from LA, might require the aid of acidic sites. The CuAl catalyst contained the most abundant acidic sites, especially Brønsted acid site, among the catalysts investigated, which was probably the reason for the higher yield of GVL at the lower reaction temperatures. To further confirm this hypothesis, D008, a commercial solid acid catalyst, was employed as a co-catalyst to catalyze the hydrogenation of LA to GVL.

The results in Entries 16 to 20 in Table 3 show that, for the CuMgAl and CuMg catalysts, the co-existence of the D008 catalyst promoted the formation of GVL, when compared with the results in Entries 11 to 15 in Table 3. Further to this, the presence of D008 catalyst also could suppress the opening of the ring in GVL to form 1,4-PDO over the CuMgAl and CuMg catalysts except the CuAl catalyst (Table 3, Entry 19), and accelerated the lactonization of 4-HVA. Nevertheless, over CuAl catalyst in the co-existence of D008 catalyst, instead of GVL, EL was produced as the main product. The

13

strong acidic sites over D008 catalyst together with the acidic sites in the CuAl catalyst were too strong to catalyze the conversion of LA to GVL, but diverted LA to EL via esterification. LTMS, a commercial Lewis acid catalyst, was also employed as the co-catalyst to catalyze the conversion of LA to GVL, as shown in Entries 21 to 25 in Table 3. Less GVL and 1,4-PDO was produced comparing with Entries 11 to 15 in Table 3, and more intermediates such as 4-HVA was observed, confirming that Brønsted acid site plays a crucial role in the lactonization of LA to GVL. Lewis acid site can not suppress the opening ring of GVL. The results herein demonstrated that the appropriate amount of Brønsted acid sites in the catalytic system was important for the effective conversion of LA to GVL. The total amounts of Brønsted acid sites need to be delicately controlled to suppress the parallel conversion of LA via esterification in especially alcohol medium. The above results also indicated that the further conversion of GVL to 1,4-PDO was favorable over the catalyst with more basic sites, as evidenced by the higher yields of 1,4-PDO over the CuMg catalyst (Table 3, Entry 10 and 15). Nevertheless, the maximum yields of 1,4-PDO was only 53.6%, further experiments were conducted to increase the yields of 1,4-PDO.

The reaction substrate and more suitable reaction medium were investigated to facilitate the opening ring of GVL to form 1,4-PDO. As shown in Table S2, isopropanol as the solvent can accelerate the opening ring of GVL and more 1,4-PDO can be obtained than that with ethanol as reaction medium, as isopropanol can be used as excellent hydrogen donor better than ethanol [45,46], which might improve hydrogenation efficiency. As for the reactants, EL, the derivatives of LA, were employed for the production of 1,4-PDO, and the products distribution was shown in Table S3. 4-hydroxyvaleric acid ethyl ester (4-HEE) was produced as intermediate from EL. EL as the reaction substrate exhibited the higher yield of 1,4-PDO under the same conditions, and thus EL was selected as the reaction substrate for further research. The detailed reason for the higher yields of 1,4-PDO from EL than from LA has not be cleared and needs further investigation.

Table 4 shows the conversion of EL versus the increasing temperature over the different catalysts. At 110°C, the main product was GVL with a small amount of 1,4-

PDO formed from the opening of the ring structure of GVL followed by the subsequent hydrogenation. The higher reaction temperature favored the opening of the ring structure of GVL to form 1,4-PDO. Further to the effects of temperature, the alkalinity of the catalysts also significantly impacted the formation of 1,4-PDO. The CuMg catalyst, which contained the highest abundance of basic sites, showed a higher yield towards 1,4-PDO production at both the low and the high temperatures. In addition, the distribution of the products showed that GVL always maintained a substantial concentration in the reaction medium. Thus, the opening of the ring structure of GVL and the subsequent hydrogenation was possibly the rate-determining step from LA or EL to 1,4-PDO. To confirm this, GVL was selected as substrate for the production of 1,4-PDO. As displayed in Table 5, the conversion of GVL to 1,4-PDO was more difficult than that from EL to GVL. Taking the CuMgAl-1-4 catalyst as an example, the conversion of GVL over this catalyst only reached 56.9% at 170ºC (Table 5, Entry 1), while the yield of GVL from EL could reach 89.4% at the temperature as low as 110ºC (Table 4, Entry 1), confirming that the rate-determining step from LA or EL to 1,4-PDO was the further conversion of GVL. In addition, the results also confirmed that CuMg showed the highest catalytic activity and selectivity towards 1,4-PDO formation, further confirming the importance of basic sites in the formation of 1,4-PDO via opening of the ring structure. Besides, GVL was also used as reactant for measuring the TOF value of different catalysts, as GVL is difficult to be further converted (conversion of GVL can be controlled below 20%). As shown in Table 1, CuMgAl-1-1 catalyst exhibits the highest TOF value than other catalysts, which can further confirm the advantages of CuMgAl-1-1 and the synergistic effect of both metal Cu sites and basic sites. Besides, MgO as external catalyst can not facilitate the opening ring of GVL as shown in Entries 11, 26 and 27 in Table 3, which also indicates that the synergistic effect between metal Cu particle and basic sites was essential rather than the mechanical mixing. To further facilitate the opening of the ring of GVL, hydrogen pressure was further taken into consideration.

As shown in Table 6, products distribution indicated that higher hydrogen pressure can efficiently accelerate the opening of the ring of GVL to form 1,4-PDO. Comparing

with Table 4 (Entries 6 to 10) and Table 6 (Entries 1 to 10), the yield of 1,4-PDO was improved with the increase of hydrogen pressure from 4 to 6 MPa, and highest yield of 1,4-PDO (98.5%) was achieved over CuMg catalyst, confirming that hydrogen pressure plays a crucial role in catalytic hydrogenation. The effects of particles size on activity were also researched, and the results are shown in Entries 1 to 5 in Table S4 as well as S5 and Fig. S6. With the increase of particles size, CuMg and CuMgAl-1-1 catalysts exhibit lower catalytic activity, when compared with the results in Entries 9 and 10 in Table 6. Highly dispersed Cu particles and fine grain should be responsible for the excellent catalytic performance to some extents. However, it is worth to note that basic sites are of great importance for high yield of 1,4-PDO comparing with CuMg-400 and CuMgAl-1-1-400 catalysts (Entries 3 and 4 in Table S4), which can also be confirmed by the TOF value (Table 1).

According to previous research [16,47], a possible reaction pathway for levulinic acid/ester was proposed in Scheme 2. During this hydrogenation process, the produced GVL was further hydrogenated to 2-hydroxy-5-methyltetrahydrofuran, which might be converted to 4-hydroxypentanal further hydrogenation to 1,4-PDO. Besides, 2-hydroxy-5-methyltetrahydrofuran might be directly converted to 1,4-PDO by the hydrogenolysis catalyzed by MgO in CuMg or CuMgAl catalysts [45], resulting in efficient catalytic activity than that over CuAl catalyst. It is worth to note that acidic sites can facilitate the abstraction of the hydrogen, which also accelerate the formation of 1,4-PDO [48].

The results obtained herein were also compared with previous work, as shown in Table S6 [10,49−52]. As for GVL production, our results demonstrated that at a lower reaction temperature and the use of non-noble metal-based catalysts, the yield of GVL could reach above 95%. With regard to 1,4-PDO production, the use of CuMg and the LDHs derived catalyst also showed comparable yields of 1,4-PDO over the noble metal-based catalyst.

3.3. Catalytic reusability

To further study the reusability of the catalysts, conversion of EL to 1,4-PDO was selected as model reaction. The results were shown in Fig. 5 (a), and the different catalysts exhibited the distinct catalytic stabilities. The CuMgAl-1-1 catalyst can maintain relatively good catalytic performance without the loss of both catalytic activities and selectivities at 170°C, as evidenced by the relatively fluctuant but stable yields of 1,4-PDO and GVL. However, the other catalysts exhibited unsatisfying selectivity to 1,4-PDO. The 1,4-PDO yield over CuAl catalysts decreased from ca. 80% to ca. 20% in the second run. The selectivity to 1,4-PDO also decreased progressively over the CuMg catalyst.

The spent catalysts were further characterized with XRD and the results are shown in Fig. 1d. These catalysts except for CuMg catalyst could maintain the crystal structure. $Mg(OH)_2$ was formed in CuMg catalyst due to the formation of water during the reaction process, indicating that CuMg catalyst was not as stable as the CuMgAl catalysts prepared with the LDHs as the precursors. As shown in Fig. S2 (f) to (h) as well as Fig. S4 (d) to (f), the SEM and TEM results of the used catalysts indicate that bigger Cu particles and more severe agglomeration of Cu grains were present in CuMg and CuAl catalysts, and EDX results (Table S1, Entries 6 to 8) indicate that Cu content did not change dramatically. Besides, XPS results of the used catalysts are shown in Table S1 and Fig. S5, and the content of Cu^+ and/or Cu^0 (932.0 and 952.0 eV) in used catalysts decreased when compared with the fresh catalysts, and the Cu $2p_{3/2}$ at ca. 933.6 eV belonged to Cu^{2+} state. Cu $2p_{1/2}$ peak at ca. 953.4 eV was attributed to the characteristic peaks of Cu^{2+} species in CuMgAl-1-1 and CuAl catalysts [35]. Therefore, abundant CuO, Cu_2O or Cu species was present in the surface of Cu-based catalysts (as sampling depth of XPS is about 3–10 nm), and it can be further reduced in liquid phase. In addition, the particle size of Cu species increased substantially for the CuMg and CuAl catalysts, while the extent of the increase of the particles size of metallic Cu in the CuMgAl catalysts was much milder. The catalysts prepared with the LDHs as precursors could inhibit the growth of metallic Cu species and maintain the catalytic activity and selectivity.

The reusability of catalysts was further researched at 140°C, and the results (Fig. 5 b) confirm that lower temperature can improve the stability of catalysts. The used catalysts were characterized by XRD, and the results are shown in Fig. S7, the growth of Cu particles was suppressed to some extents. The stability of CuAl catalyst was still worse than CuMg and CuMgAl catalysts.

4. Conclusions

In summary, the Cu-based catalysts produced via the LDH precursors with the distinct distribution of acidic sites and basic sites substantially impacted physiochemical properties and the selectivity of GVL or to 1,4-PDO from levulinic acid/ester. The presence of Mg in the CuMgAl catalyst could enhance the development of the porous structures of the catalyst, the reduction of the particle sizes of Cu species, while alleviate the interaction between CuO and alumina. Further to this, the introduction of Mg increased the abundance of basic sites on surface of the catalysts, which remarkably impacted the catalytic selectivity towards GVL to form 1,4-PDO. The results herein demonstrated that the abundant acidic sites over the CuAl catalyst, especially Brønsted acid site, could suppress the opening of the ring of GVL, achieving a high selectivity towards GVL, while suppressing the production of 1,4-PDO. Nevertheless, the total amounts of acidic sites also need to be delicately controlled to suppress the esterification of LA, the competitive reaction for the conversion from LA to GVL. In addition, the basic sites on the surface of catalyst promoted the conversion of GVL to 1,4-PDO via the opening of the ring structure of GVL, the rate-determining step from LA or EL to 1,4-PDO. Hence, high yield of GVL was obtained over the catalyst with abundant Brønsted acidic sites, while high yield of 1,4-PDO was obtained over the catalyst with abundant basic sites and highly dispersed copper sites. The recyclability tests showed that the CuMgAl catalyst could maintain the catalytic stability, while the CuMg or CuAl catalyst could not. The formation of $Mg(OH)_2$ in CuMg catalyst changed the crystal structure of the catalyst, while the crystal size of metallic Cu species in either CuMg or CuAl catalyst increased substantially. Lower reaction temperature and higher reaction hydrogen pressure can effectively improve the

stability of catalysts and suppress the growth of Cu particles to some extent. The CuMgAl catalyst prepared with the LDHs precursors could inhibit the growth of metallic Cu species and maintained the catalytic activity and selectivity. The CuMgAl catalyst with the tunable acid-base properties is also expected to tune the catalytic selectivity to the targeting products in other reaction systems.

Acknowledgements

References

1. A. Gupta, J. P. Verma, Renew. Sust. Energ. Rev., 2015, 41, 550.

2. N. Gaurav, S. Sivasankari, G. S. Kiran, A. Ninawe, J. Selvin, Renew. Sust. Energ. Rev., 2017, 73, 205.

3. X. Hu, S. J. Jiang, L. P. Wu, S. Wang, C.-Z. Li, Chem. Commun., 2017, 53, 2938.

4. X. Hu, R. J. M. Westerhof, L. P. Wu, D. H. Dong, C.-Z. Li, Green Chem. 2015, 17, 219.

5. K. Yan, C. Jarvis, J. Gu, Y. Yan, Renew. Sust. Energ. Rev., 2015, 51, 986.

6. Y. W. Shao, X, Hu, Z. M. Zhang, K. Sun, G. G. Gao, T. Wei, S. Zhang, S. Hu, J. Xiang, Y. Wang, Green Energy Environ., In press, 2018.

7. F. G. Cirujano, A. Corma, F. X. Llabrés i Xamena, Chem. Eng. Sci., 2015, 124, 52.

8. C. Xie, J. L. Song, B. W. Zhou, J. Y. Hu, Z. R. Zhang, P. Zhang, Z. W. Jiang, B. X. Han, ACS Sustain.Chem. Eng., 2016, 4, 6231.

9. S. Dutta, I. K. M. Yu, D. C. W. Tsang, Y. H. Ng, Y. S. Ok, J. Sherwood, J. H. Clark, Chem. Eng. J., 2019, 372, 992.

10. T. Mizugaki, Y. Nagatsu, K. Togo, Z. Maeno, T. Mitsudome, K. Jitsukawa, K. Kaneda, Green Chem., 2015, 17, 5136.

11. J. L. Cui, J. J. Tan, Y. L. Zhu, F. Q. Cheng, ChemSusChem, 2018, 11, 1316.

12. F. D. Pileidis, M. M. Titirici, ChemSusChem, 2016, 9, 562.

13. R. S. Varma, ACS Sustain. Chem. Eng., 2019, 7, 6458.

14. D. Q. Ding, J. J. Wang, J. X. Xi, X. H. Liu, G. Z. Lu, Y. Q. Wang, Green Chem., 2014, 16, 3846.

15. H. C. Zhou, J. L. Song, X. C. Kang, J. Y. Hu, Y. Y. Yang, H. L. Fan, Q. L. Meng, B. X. Han, RSC Adv., 2015, 5, 15267.

16. D. Z. Ren, X. Y. Wan, F. M. Jin, Z. Y. Song, Y. J. Liu, Z. B. Huo, Green Chem., 2016, 18, 5999.

17. U. Omoruyi, S. Page, J. Hallett, P. W. Miller, 2016, ChemSusChem, 9, 2037.

18. O. Mamun, E. Walker, M. Faheem, J. Q. Bond, A. Heyden., ACS Catal., 2016, 7, 215.

Green Chemistry Accepted Manuscript

19. P. P. Upare, M. Lee, S. -K. Lee, J. W. Yoon, J. Bae, D. W. Hwang, U. -H. Lee, J. -S. Chang, Y. K. Hwang, Catal. Today, 2016, 265, 174.

20. Q. Xu, X. L. Li, T. Pan, C. G. Yu, J. Deng, Q. X. Guo, Y. Fu, Green Chem., 2016, 18, 1287.

21. J. L. Song, L. Q. Wu, B. W. Zhou, H. C. Zhou, H. L. Fan, Y. Y. Yang, Q. L. Meng, B. X. Han, Green Chem., 2015, 17, 1626.

22. P. P. Upare, M. -G. Jeong, Y. K. Hwang, D. H. Kim, Y. D. Kim, D. W. Hwang, U. H. Lee, J. -S. Chang, Appl. Catal. A: Gen., 2015, 491, 127.

23. Y. Yang, G. Gao, X. Zhang, F. W. Li, ACS catal. 2014, 4, 1419.

24. H. C. Zhou, J. L. Song, H. L. Fan, B. B. Zhang, Y. Y. Yang, J. Y. Hu, Q. G. Zhu, B. X. Han, Green Chem., 2014, 16, 3870.

25. X. D. Long, P. Sun, Z. L. Li, R. Lang, C. G. Xia, F. W. Li, Chinese J. Catal., 2015, 36, 1512.

26. S. Song, S. K. Yao, J. H. Cao, L. Di, G. J. Wu, N. J. Guan, L. D. Li, Appl. Catal. B: Environ., 2017, 217, 115.

27. J. Zhang, J. Z. Chen, Y. Y. Guo, L. M. Chen, ACS Sustain. Chem. Eng., 2015, 3, 1708.

28. J. Wu, G. Gao, Y. Li, P. Sun, J. Wang, F. W. Li, Appl. Catal. B: Environ., 2019, 245, 251.

29. C. X. Xiao, T. -W. Goh, Z. Y. Qi, S. Goes, K. Brashler, C. Perez, W. Y. Huang, ACS Catal., 2015, 6, 593.

30. J. J. Tan, J. L. Cui, T. S. Deng, X. J. Cui, G. Q. Ding, Y. L. Zhu, Y. W. Li, ChemCatChem, 2015, 7, 508.

31. D. L. Sun, A. Ohkubo, K. Asami, T. Katori, Y. Yamada, S. Sato, Mol. Catal., 2017, 437, 105.

32. K. Hengst, M. Schubert, H. W. P. Carvalho, C. B. Lu, W. Kleist, J. -D. Grunwaldt, Appl. Catal. A, Gen., 2015, 502, 18.

33. B. Cai, X. C. Zhou, Y. C. Miao, J. Y. Luo, H. Pan, Y. B. Huang, ACS Sustain. Chem. Eng., 2017, 5, 1322.

34. Z. Cao, J. H. Bu, Z. Q. Zhong, C. Y. Sun, Q. S. Zhang, J. D. Wang, S. H. Chen, X. W. Xie, Appl. Catal. A, Gen., 2019, 578, 105.

35. G. Q. Cui, X. Y. Meng, X. Zhang, W. L. Wang, S. L. Xu, Y. C. Ye, K. J. Tang, W. M. Wang, J. H. Zhu, M. Wei, D. G. Evans, X. Duan, Appl. Catal. B: Environ., 2019, 248, 394.

36. Y. Y. Cao, L. B. Niu, X. Wen, W. H. Feng, L. Huo, G. Y. Bai, J. Catal., 2016, 339, 9.

37. M. M. Li, Y. Li, L. Jia, Y. Wang, Catal. Commun., 2018, 103, 88.

38. Y. W. Shao, K. Sun, Q. Y. Li, L. J. Zhang, T. Wei, G. G. Gao, S. Zhang, Y. Wang, Q. Liu, X. Hu, Bioresource Technol. Rep., 2019, 100218.

39. X. Y. Lin, R. L. Li, M. M. Lu, C. Q. Chen, D. L. Li, Y. Y. Zhan, L. L. Jiang, Fuel, 2015, 162, 271.

40. J. L. Eslava, X. H. Sun, J. Gascon, F. Kapteijn, I. Rodríguez-Ramos, Catal. Sci. Technol., 2017, 7, 1235.

41. H. Meng, J. N. Liu, Y. L. Du, B. H. Hou, X. Wu, X. M. Xie, Catal. Commun., 2019, 119, 101.

42. C. W. Dong, C. L. Yin, T. T. Wu, Z. Y. Wu, D. Liu, C. G. Liu, Catal. Commun., 2019, 119, 164.

43. X, Jiao, L. Li, H. G. Li, F. K. Xiao, N. Zhao, W. Wei, B. S. Zhang, Mater. Res. Bull. 2015, 64, 163.

44. L. L. Negahdar, M. G. Al-Shaal, F. J. Holzhäuser, R. Palkovits, Chem. Eng. Sci., 2017, 158, 545.

45. D. Wang, C. Deraedt, J. Ruiz, D. Astruc, J. Mol. Catal. A, Chem., 2015, 400, 14.

46. M. J. Gilkey, B. Xu, ACS catal., 2016, 6, 1420.

47. U. Omoruyi, S. Page, J. Hallett, P. W. Miller, ChemSusChem, 2016, 9, 2037.

48. S. C. Patankar, G. D. Yadav, ACS Sustain. Chem. Eng., 2015, 3, 2619.

49. K. Hengst, M. Schubert, H. W. P. Carvalho, C. B. Lu, W. Kleist, J. D, Appl. Catal. A, Gen., 2015, 502, 18.

50. K. Hengst, M. Schubert, H. W. P. Carvalho, C. B. Lu, W. Kleist, J.-D. Grunwaldt, 2015, 502, 18.

51. J. Zhang, J. Z. Chen, Y. Y. Guo, L. M. Chen, ACS Sustain. Chem. Eng., 2015, 3, 1708.

52. K. Jiang, D. Sheng, Z. H. Zhang, J. Fu, Z. Y. Hou, X. Y. Lu, Catal. Today, 2016, 274, 55.

Green Chemistry Accepted Manuscript
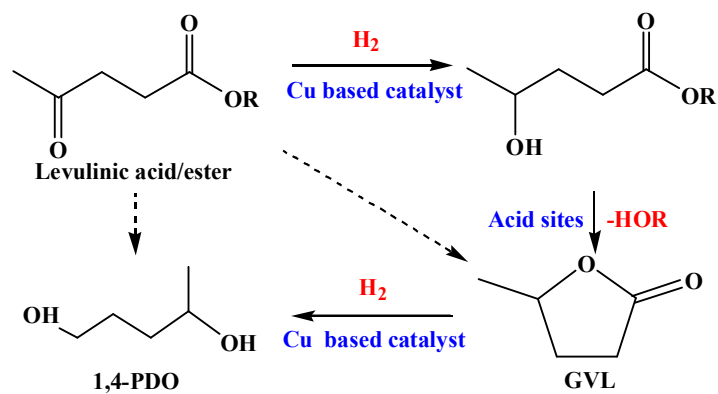
Scheme 1 Conversion of levulinic acid/ester to GVL and 1,4-PDO. All compounds in this scheme were detected with GC-MS.
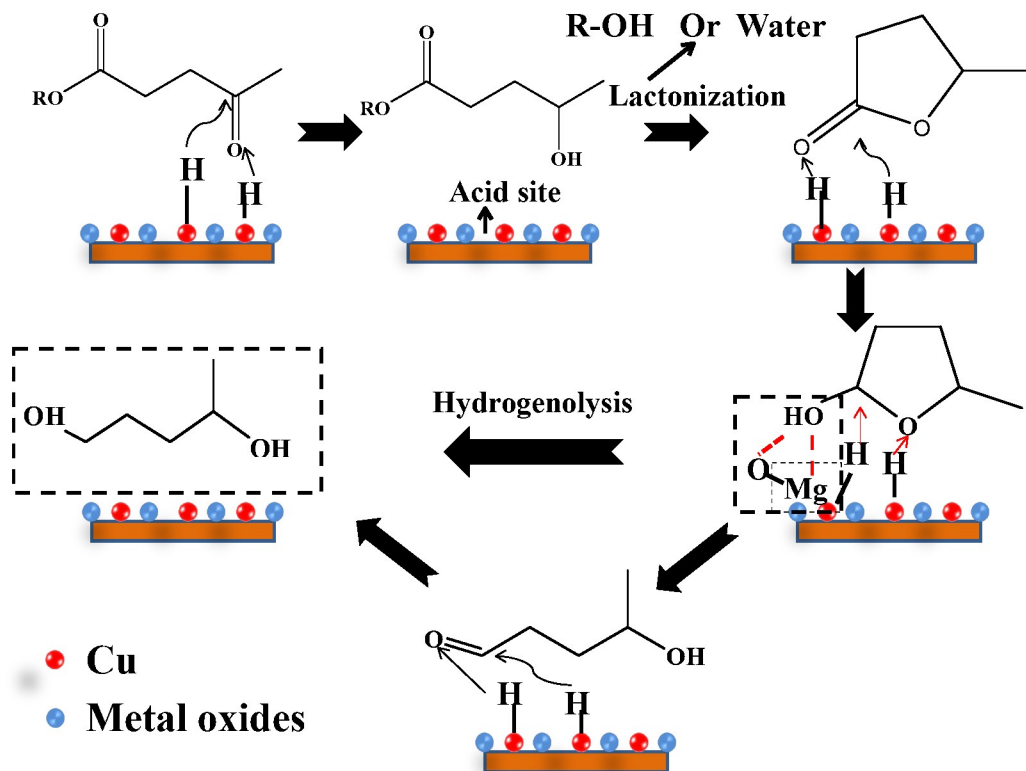
Scheme 2 The proposed reaction pathways for hydrogenation of levulinic acid/ester to GVL and 1,4-PDO.

Table 1 Textural property of calcined Cu-based catalysts and Cu particle size of fresh and spent Cu-based catalysts

Entry	Catalysts	BET surface area[a] (m²/g)	Pore volume[a] (cm³/g)	Pore size[a] (nm)	Cu particle size[b] (nm) Fresh	Cu particle size[b] (nm) Spent	D[c]$_{Cu}$ (%)	S[c]$_{Cu}$ (m² g⁻¹)	TOF[d] (h⁻¹)
1	CuAl	50.4	0.37	14.6	12.9	17.5	12.8	37.7	3.9
2	CuMgAl-1-4	89.4	0.57	12.8	4.5	−	63.3	69.2	1.1
3	CuMgAl-1-2	103.4	0.71	13.7	4.7	−	25.1	40.8	2.4
4	CuMgAl-1-1	97.9	0.71	14.6	5.5	6.5	23.3	66.2	6.2
5	CuMg	92.8	0.71	15.4	4.1	11.3	22.6	61.6	5.0

[a]BET surface area, pore volume and average pore size were measured by N_2 adsorption-desorption.

[b]Cu particle size was calculated by the Debye-Scherrer equation based on XRD.

[c]Surface Cu particle dispersion (D_{Cu}) and surface area (S_{Cu}) were determined by N_2O chemisorptions.
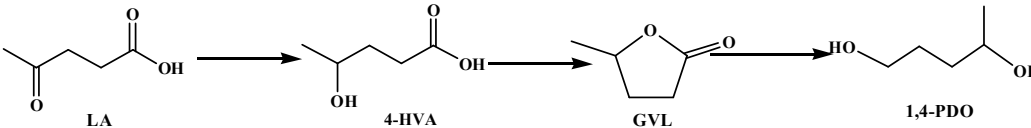
[d]TOF is calculated with GVL as the reactant.

Table 2 The acidic/basic distribution of CuMgAl, CuMg and CuAl catalysts

Entry	Catalysts	Acidic sites (µmol/g)				Basic sites (mmol/g)			
		AWa	AM	AS	AT	BWb	BM	BS	BT
1	CuAl	8.8	23.6	26.6	58.9	52.1	10.2	22.2	84.6
2	CuMgAl-1-4	5.1	12.6	34.8	52.6	69.8	51.2	150.1	271.1
3	CuMgAl-1-2	6.6	12.7	39.3	58.6	58.5	51.4	106.8	216.8
4	CuMgAl-1-1	7.6	10.0	17.1	34.6	93.8	65.0	124.2	283.1
5	CuMg	14.2	5.7	9.1	29.0	74.2	106.7	173.2	354.1

[a]AW represents the concentration of weak Brønsted acid site; AM represents the concentration of moderate Lewis acid site; AS represents the concentration of strong Lewis acid site; AT represents the concentration of total acid sites.

[b]BW represents the concentration of weak Brønsted base site; BM represents the concentration of moderate Lewis base site; BS represents the concentration of strong Lewis base site; BT represents the concentration of total base site.

Table 3 Distribution of the products in hydrogenation of LA in ethanol[a]

| Entry | T (°C) | Catalysts | Con. (%) | Yield (%) | | Carbon balance (%) |
				GVL	1,4-PDO	
1	110	CuAl	100.0	95.3	–	> 95.3
2	110	CuMgAl-1-4	100.0	86.5	–	> 86.5
3	110	CuMgAl-1-2	100.0	85.2	–	> 85.2
4	110	CuMgAl-1-1	100.0	85.8	–	> 85.8
5	110	CuMg	100.0	84.9	–	> 84.9
6	140	CuAl	100.0	88.1	2.2	> 90.3
7	140	CuMgAl-1-4	100.0	80.9	1.9	> 82.8
8	140	CuMgAl-1-2	100.0	76.6	4.7	> 81.3
9	140	CuMgAl-1-1	100.0	78.2	5.3	> 83.5
10	140	CuMg	100.0	73.7	15.3	> 89.0
11	170	CuAl	100.0	68.7	22.7	> 91.4
12	170	CuMgAl-1-4	100.0	66.1	18.5	> 84.6
13	170	CuMgAl-1-2	100.0	64.3	22.0	> 86.3
14	170	CuMgAl-1-1	100.0	59.2	28.0	> 87.2
15	170	CuMg	100.0	39.7	53.6	> 93.3
16	170	CuAl+D008	100.0	97.8[b]	0.0	> 97.8
17	170	CuMgAl-1-4+D008	100.0	89.4	4.7	> 94.1
18	170	CuMgAl-1-2+D008	100.0	85.5	11.6	> 97.1
19	170	CuMgAl-1-1+D008	100.0	80.2	16.4	> 96.6
20	170	CuMg+D008	100.0	67.3	26.2	> 93.5
21	170	CuAl+LTMS	100.0	55.2	1.5	> 56.7
22	170	CuMgAl-1-4+ LTMS	100.0	65.2	12.4	> 77.6
23	170	CuMgAl-1-2+ LTMS	100.0	59.3	20.9	> 80.2
24	170	CuMgAl-1-1+ LTMS	100.0	46.9	36.6	> 83.5
25	170	CuMg+ LTMS	100.0	43.6	36.1	> 79.7
26	170	CuAl+MgO[c]	100.0	68.2	11.4	> 79.6
27	170	CuAl+MgO[d]	100.0	70.5	10.3	> 80.8

[a]Reaction conditions: t = 2 h; P_{H2} = 3 MPa (at room temperature); stirring speed = 400 rpm; catalyst loading: 40 mg; reactant loading: 40 mg; ethanol: 3.96 g, D008 = 40 mg; LTMS = 20 mg.

[b]The yield of EL.

[c]MgO = 20 mg.

[d]MgO = 40 mg.

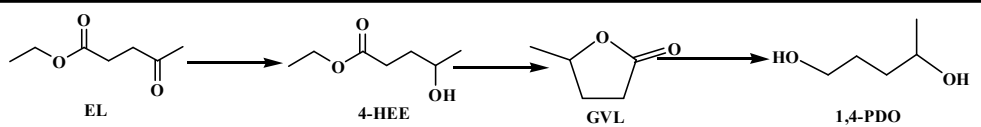**Table 4** Distribution of the products in hydrogenation of EL in isopropanol[a]

Entry	T (°C)	Catalysts	Con. (%)	Yield (%)		Carbon balance (%)
				GVL	1,4-PDO	
1	110	CuAl	100.0	85.9	8.3	> 94.2
2	110	CuMgAl-1-4	100.0	89.4	4.7	> 94.1
3	110	CuMgAl-1-2	100.0	85.5	11.6	> 97.1
4	110	CuMgAl-1-1	100.0	80.2	16.4	> 96.6
5	110	CuMg	100.0	69.0	25.3	> 94.3
6	140	CuAl	100.0	52.4	40.5	> 92.9
7	140	CuMgAl-1-4	100.0	64.6	27.1	> 91.7
8	140	CuMgAl-1-2	100.0	37.0	57.0	> 94.0
9	140	CuMgAl-1-1	100.0	31.3	64.3	> 95.6
10	140	CuMg	100.0	16.5	81.2	> 97.7
11	170	CuAl	100.0	16.7	80.3	> 97.0
12	170	CuMgAl-1-4	100.0	13.8	83.7	> 97.5
13	170	CuMgAl-1-2	100.0	12.7	85.7	> 98.4
14	170	CuMgAl-1-1	100.0	6.9	91.5	> 98.4
15	170	CuMg	100.0	7.2	91.4	> 98.6

[a]Reaction conditions: t = 3 h; P_{H2} = 4.0 MPa (at room temperature); stirring speed = 400 rpm; catalyst loading: 40 mg; reactant loading: 40 mg; isopropanol: 3.96 g.

Table 5 Distribution of the products in hydrogenation of GVL in isopropanol[a]

Entry	Catalyst	Con. (%)	1,4-PDO	
			Yield (%)	Selectivity (%)
1	CuAl	76.2	71.4	93.7
2	CuMgAl-1-4	56.9	48.5	85.2
3	CuMgAl-1-2	86.8	83.7	96.4
4	CuMgAl-1-1	89.9	87.4	97.2
5	CuMg	92.4	90.1	97.5

[a]Reaction conditions: temperature = 170°C; t = 2 h; P_{H2} = 4 MPa (at room temperature);

stirring speed = 400 rpm; catalyst loading: 40 mg; reactant loading: 40 mg; isopropanol:

3.96 g.

Table 6 Distribution of the products in hydrogenation of EL in isopropanol[a]

Entry	P_{H2} (MPa)	Catalysts	Con. (%)	Yield (%)		Carbon balance (%)
				GVL	1,4-PDO	
1	5.0	CuAl	100.0	42.0	51.5	> 93.5
2	5.0	CuMgAl-1-4	100.0	65.9	25.7	> 91.6
3	5.0	CuMgAl-1-2	100.0	32.0	62.2	> 94.2
4	5.0	CuMgAl-1-1	100.0	6.7	90.9	> 97.6
5	5.0	CuMg	100.0	1.6	96.6	> 98.2
6	6.0	CuAl	100.0	16.1	81.4	> 97.5
7	6.0	CuMgAl-1-4	100.0	55.4	37.0	> 92.4
8	6.0	CuMgAl-1-2	100.0	20.3	76.7	> 97.0
9	6.0	CuMgAl-1-1	100.0	3.0	96.7	> 99.7
10	6.0	CuMg	100.0	1.1	98.5	> 99.6

[a]Reaction conditions: t = 3 h; T = 140°C; stirring speed = 400 rpm; catalyst loading: 40 mg; reactant loading: 40 mg; isopropanol: 3.96 g.
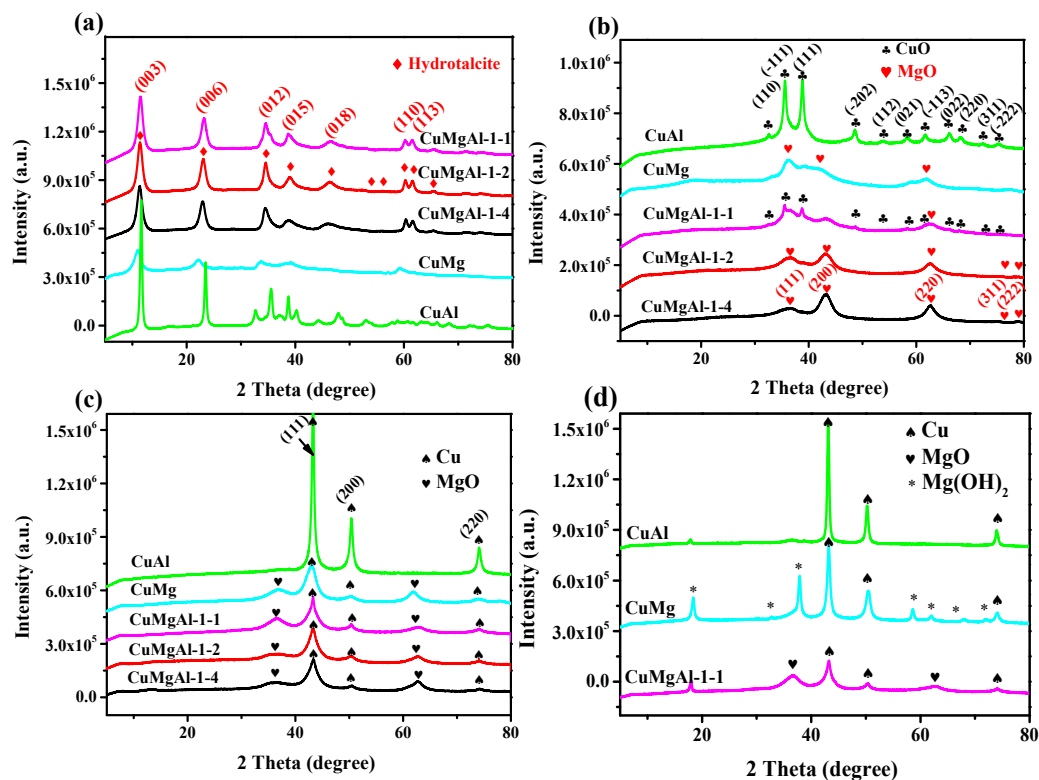
Fig. 1 XRD patterns of Cu-based catalysts: (a) hydrotalcite structure before calcination;

(b) after calcination; (c) after reduction; (d) after cycle experiment.
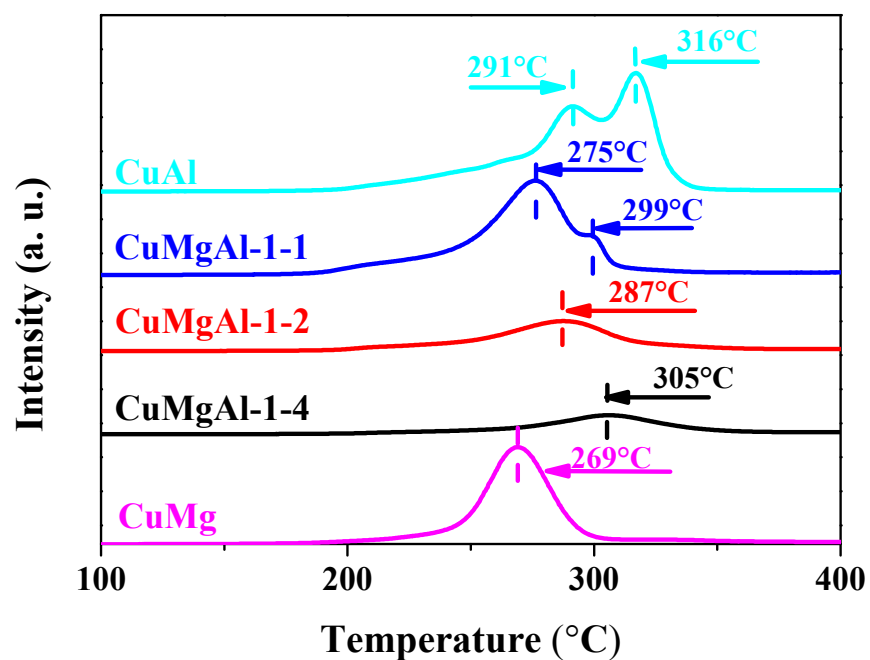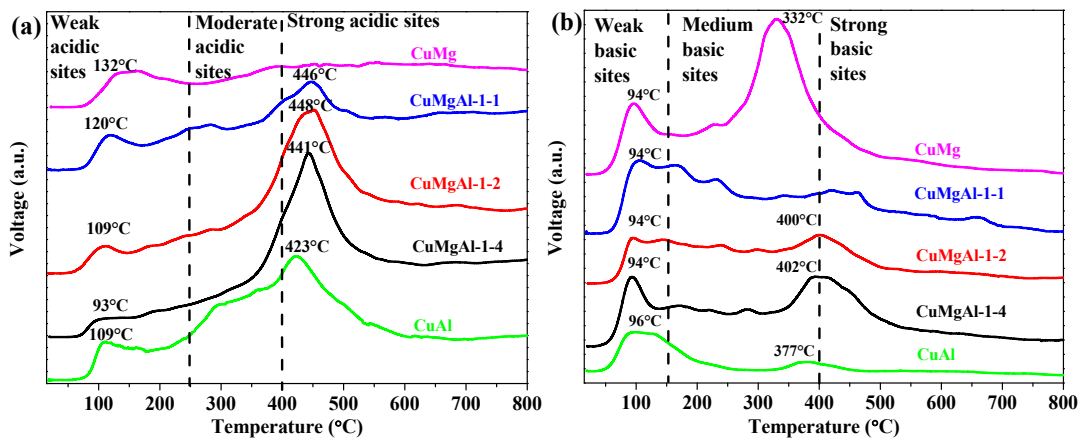
Fig. 2 H$_2$−TPR profiles of the copper-based catalysts.

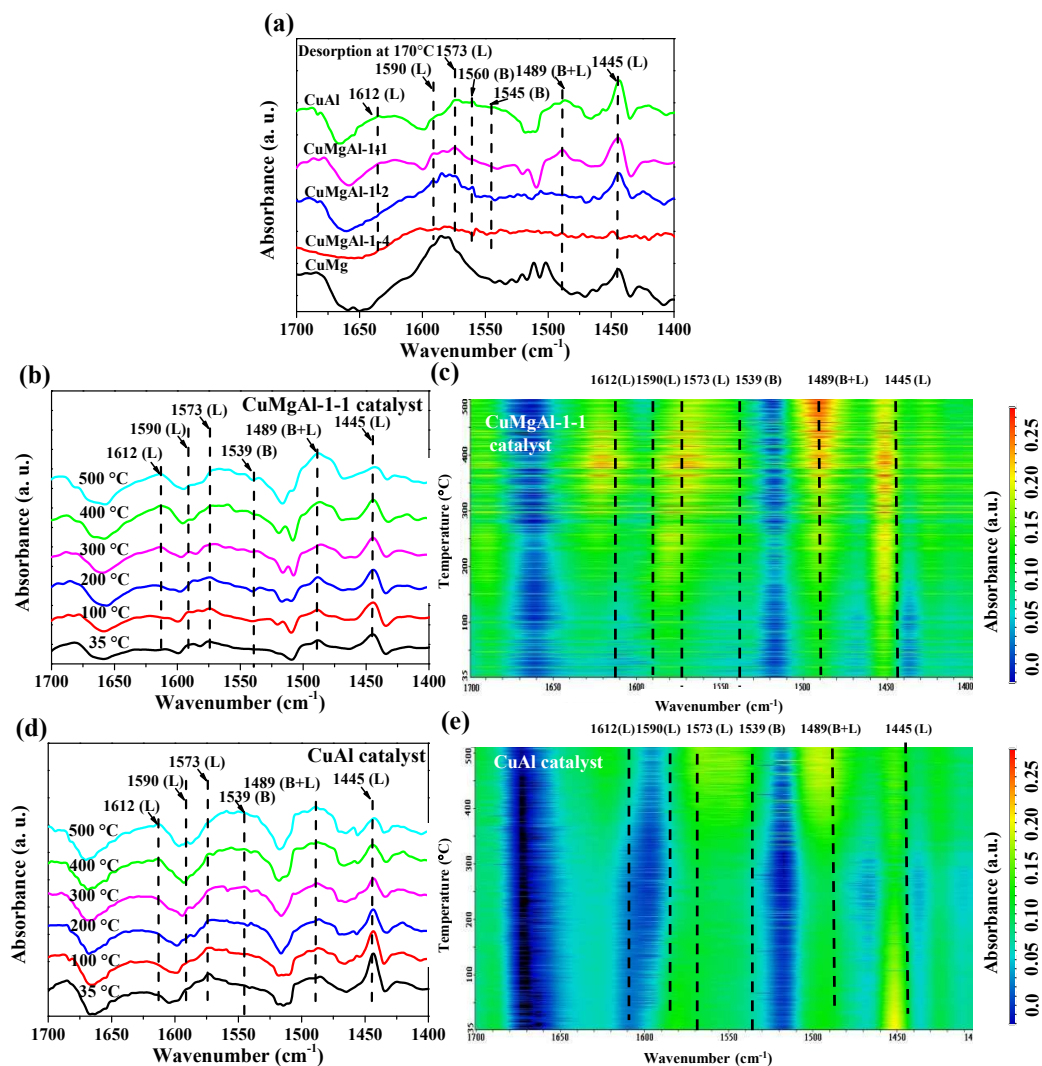**Fig. 3** NH$_3$–TPD (a) and CO$_2$–TPD (b) curves of the copper-based catalysts.

Fig. 4 (a) *In situ* FTIR spectra of pyridine on various samples at 170°C; (b) to (c) and (d) to (e) *In situ* FTIR spectra of pyridine on CuMgAl-1-1 and CuAl catalysts at different temperatures.
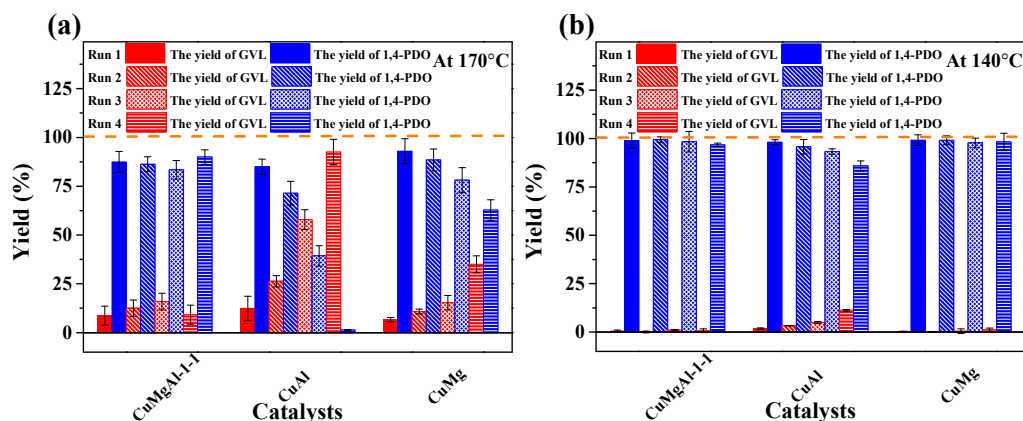
Fig. 5 Recycle tests of hydrogenation of EL in isopropanol over the different catalysts at (a) 170°C and (b) 140°C. (a) Reaction conditions: t = 4 h; P_{H2} = 4 MPa (at room temperature); stirring speed = 400 rpm; catalyst loading: 80 mg; reactant loading: 40 mg; isopropanol: 3.96 g. (b) Reaction conditions: t = 6 h; P_{H2} = 6 MPa (at room temperature); stirring speed = 400 rpm; catalyst loading: 80 mg; reactant loading: 40 mg; isopropanol: 3.96 g.